Chapter

Structure Analysis of Quasicrystal Approximants by Rotation Electron Diffraction (RED)

Devinder Singh and Sven Hovmöller

Abstract

Complete 3D electron diffraction can be collected by rotation electron diffraction (RED) for single-crystal powder-sized samples, i.e., <0.1 μm, in all dimensions. Data collection takes about 1 h and data processing takes another hour. The crystal structures are solved by standard crystallographic techniques. X-ray crystallography requires crystals several micrometers big. For nanometer-sized crystals, electron diffraction and electron microscopy (EM) are the only possibilities. Two methods have been developed for collecting complete (except for a missing cone) three-dimensional (3D) electron diffraction data: the rotation electron diffraction and automated electron diffraction tomography (ADT). By collecting 1000–2000 electron diffraction patterns, a complete 3D data set is obtained. The geometry in RED is analogous to the rotation method in X-ray crystallography; the sample is rotated continuously along one rotation axis. In recent years, large number of crystal structures has been solved by RED. These include the most complex zeolites ever solved and quasicrystal approximants, such as the pseudo-decagonal approximants PD2 and PD1 in Al-Co-Ni. In this chapter, the results of our recent studies on the structure analysis of complex pseudo-decagonal (PD) quasicrystal approximants PD2 (a = 23.2, b = 32.3, c = 4.1 Å) and PD1 (a = 37.3, b = 38.8, c = 4.1 Å) by RED have been discussed. These are known to be the most complicated approximant structures ever solved to atomic resolution by electron crystallography. PD2 and PD1 are built of characteristic 2 nm wheel clusters with fivefold rotational symmetry, which agrees with other approximants in the PD series as well as with the results from high-resolution electron microscopy images.

Keywords: electron crystallography, rotation electron diffraction, quasicrystal, approximant

1. Introduction

One of the most important techniques for studying crystals is electron crystallography. Recently, a new method, rotation electron diffraction (RED), has been developed for collecting three-dimensional (3D) electron diffraction data by combining electron beam tilt and goniometer tilt in a transmission electron microscope [1–4]. RED is capable of structure determination as well as phase identification of unknown crystals. It is easier, much faster, and more straightforward than powder X-ray diffraction and other electron microscopy techniques, such as high-resolution

transmission electron microscopy (HRTEM). There is no enigma in the determination of unit cell, space group and indexing of diffraction peaks in RED [5].

The low-density structures such as zeolites and open-framework compounds are solved by RED method [5, 6]. Since, complex dense intermetallic compounds such as quasicrystal approximants contain heavy elements and thus suffer more from dynamical scattering, it is interesting to see if they can also be solved from RED data. Quasicrystals possess aperiodic long-range order associated with crystallographically forbidden rotational symmetries (5-, 8-, 10-, or 12-fold) and exhibit many outstanding physical properties [7–13]. Several breakthrough experiments performed by Dan Shechtman in 1982 on rapidly solidified Al-Mn alloys have led to the discovery of quasicrystals. It exhibits sharp diffraction peaks with icosahedral symmetry [14]. Quasicrystals exhibit unique physical properties which strongly differ from the properties of metals, insulators, and crystalline or amorphous phases [7–13, 15–21]. Thus, these materials have the potential to be used in many areas of advanced technology. Out of the many alloy systems which possess quasicrystalline phases, Al-based quasicrystalline alloy systems are easily available, cheap, and non-toxic.

The most critical aspect of quasicrystals from the experimental and theoretical point of view is to solve their structures. Their structures have been solved theoretically using a sequence of periodic structures with growing unit cells [22–24]. There exist also a number of crystalline phases resembling the quasicrystals, known as approximant phases [22]. The diffraction patterns of approximant phases are closely related to those of quasicrystals as their structures are built up by the same clusters as in quasicrystals. Quasicrystals and their approximant phases have similar electron diffraction patterns and chemical compositions [25–31], showing that they have similar local structures. One approach is to determine the structures of approximants. This helps us to get a deep understanding of the relationships between quasicrystals and their approximant phases. Thus, approximant phases may hold the key to determine the structures of quasicrystals.

The HRTEM and high-angle annular dark-field (HAADF) studies of Al-Co-Ni decagonal quasicrystals suggest that the basic structure is composed of 2 nm clusters with fivefold rotational symmetry [32–34]. A series of pseudo-decagonal (PD) quasicrystal approximants in Al-Co-Ni with almost 10-fold symmetry of their electron diffraction patterns have been found and described [35, 36]. Out of those approximants, only two structures, namely, PD4 [37] and PD8 (also called the W-phase) [38], have been solved to atomic resolution by X-ray crystallography. The PD1, PD2, PD3, and PD5 structures were solved at low resolution from the limited information provided by electron diffraction patterns, unit cell dimensions, and HRTEM images [39]. An attempt to solve the structures of PD1 and PD2 in $Al_{71}Co_{14.5}Ni_{14.5}$ alloy by maximum entropy Patterson deconvolution was reported by Estermann et al. [40]. Since these two structures were found to intergrow, thus there was a serious problem in the application of X-ray diffraction. This problem can be eliminated in the case of electron crystallography as much smaller crystals ($<1\ mm^3$) are needed for electron diffraction. Recently, we have solved the structures of PD2 and PD1 by RED method [41, 42]. The present chapter deals with the results and discussion of these two structures.

The decagonal quasicrystals are described by a quasiperiodic arrangement of clusters [43–46]. All decagonal quasicrystals in Al-Co-Ni and their high-order approximants are composed of 2 nm wheel clusters [47–51]. The arrangement of atoms within the clusters imposes restrictions on the cluster arrangements, e.g., an overlapping of clusters [52–56]. To understand the structure of quasicrystals, it is important to find the details of the atomic arrangements within the 2 nm wheel clusters and their packing into a 3D crystal. The geometrical building principles of

Al-Co-Ni, Al-Co-Cu, and Al-Fe-Ni decagonal quasicrystals and their approximant phases in terms of a fundamental unit cluster-based approach that leads to a unifying view of all these phases have been discussed [57]. This unit cluster has ~2 nm diameter.

The RED method has been applied for ab initio structure determination of PD2 (a = 23.2, b = 32.3, c = 4.1 Å) and PD1 (a = 37.3, b = 38.8, c = 4.1 Å), quasicrystal approximants in the Al–Co–Ni alloy system, and their structure determination by direct methods from the RED data set. After PD8 (a = 23.2, b = 19.8, c = 4.1 Å), PD2 has the second smallest unit cell area in the PD series [39]. a = 23.2 Å is the same as that for PD8, but b is τ (the golden mean 1.61803. ..) times larger than 19.8 Å, i.e., 32.0 Å, the same as that in PD4 (a = 101.3, b = 32.0, c = 4.1 Å). Compared with PD2 and PD8, PD1 has a larger unit cell and hence contains more atoms. Solving the structures of more complex quasicrystal approximants in the PD series from electron diffraction data by direct methods will be more challenging, because of the increased unit cell dimensions and number of unique atoms in the unit cell.

2. Materials and experimental procedure

The details of the preparation methods of $Al_{71}Co_{14.5}Ni_{14.5}$ nominal composition are reported elsewhere [41, 42]. Powder X-ray diffraction examination revealed a diffraction pattern typical of PDs [35]. A piece of the annealed sample was powdered and dispersed in ethanol and treated by ultrasonification for 2 min. A droplet of the suspension was transferred onto a copper grid (with carbon film). The 3D-RED data were collected on a JEOL JEM-2100 LaB6 microscope at 200 kV [1]. The single-tilt tomography sample holder was used for data collection. In RED, we combine electron beam tilt and goniometer tilt (**Figure 1**). The RED data collection software package was used which controls 3D-RED data collection in an automated way [1, 4, 58]. The selected area diffraction patterns were collected at each tilt angle from a μm-sized crystal (**Figure 1(b)**). For RED data collection, electron beam tilt with many small steps and goniometer tilt with larger steps was combined to cover

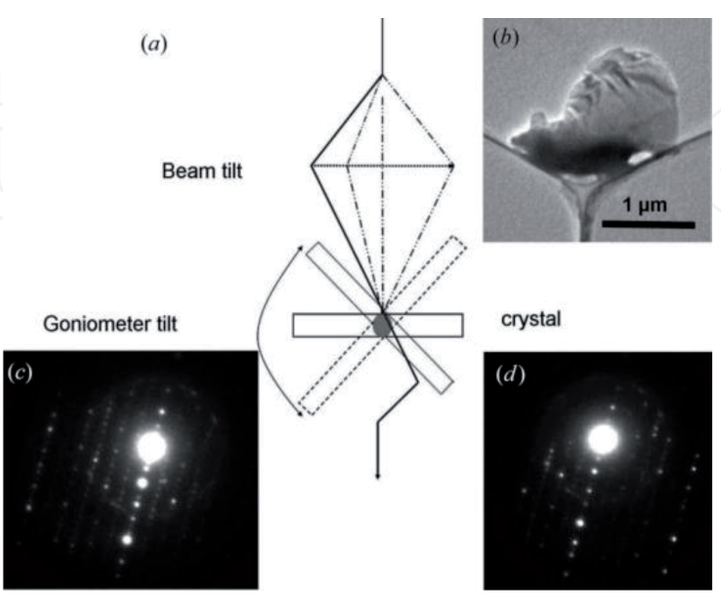

Figure 1.
(a) Ray diagram of the electron beam rotation, showing beam tilt and goniometer tilt. (b) a single crystal of size ~2.0 × 1.0 × <0.1 mm was used for the RED data collection. (c) and (d) two diffraction patterns of PD2 which are 1.0° (20 frames) apart. Reproduced with permission of the International Union of Crystallography (https://scripts.iucr.org/cgi-bin/paper?HE5621) [41].

a large part of reciprocal space. **Table 1** gives the details of the RED data collection and crystallographic information for the PD2 and PD1 quasicrystal approximants. Energy-dispersive spectroscopy (EDS) analysis was carried out on the same crystal after the RED data collection which showed that the composition was close to the nominal one.

The software package RED data processing was used for the data processing of the collected frames [4, 58], including direct beam-shift correction, peak search, unit cell determination, indexing of reflections, and intensity extraction. ED frames collected were combined into a 3D data set for reciprocal space reconstruction. After reciprocal space had been reconstructed, the unit cell parameters, space group, reflection indices, and diffraction intensities were determined. The indexing

Name	**Pseudo-decagonal (PD2) quasicrystal approximant**	**Pseudo-decagonal (PD1) quasicrystal approximant**
Chemical formula	$Al_{37}(Co,Ni)_{15.5}$	$Al_{77}(Co/Ni)_{31}$
Temperature (K)	298	298
Wavelength (Å)	0.02508	0.02508
Crystal system	Orthorhombic	Orthorhombic
Space group	*Pnmm*	*Pnam*
Unit cell parameters (Å)	a = 23.2, b = 32.3, c = 4.1	a = 37.3, b = 38.8, c = 4.1
Volume (Å^3)	3075.7	5933.68
Density (calculated in Mg cm^{-3})	4.132	4.374
Crystal size (μm)	2.0 × 1.0 × <0.1	2.0 × 2.0 × <0.1
Tilt range (°)	−74.3 to +36.0	+29.5 to −64.6
Tilt step (°)	0.05	0.05
Exposure time/frame (s)	0.5	0.2
Total data collection time (min)	90	90
No. of frames	2255	2050
Program for structure determination	*SHELX97*	*SHELX97*
Resolution (Å)	1.0	1.0
Completeness (%)	89.3	94.5
Reflections collected	8153	7070
R(int)	0.33	0.26
Observed unique reflections ($I > 2\sigma$)	1799	2588
Parameters/restraints	156 with 0 restraint	325 with 0 restraint
Goodness-of-fit on F^2	4.155	2.854
Final R indices ($I > 2\sigma$)	R_1 = 0.4285, wR_2 = 0.7023	R_1 = 0.3606, wR_2 = 0.6641
R (all reflections)	0.4326	0.3671
Highest peak and deepest hole	1.98 and − 2.56	1.31 and − 1.42

Reproduced with permission of the International Union of Crystallography (https://scripts.iucr.org/cgi-bin/paper?HE5621 & https://scripts.iucr.org/cgi-bin/paper?jo5016) [41, 42].

Table 1.
Crystallographic data, RED experimental parameters, and structure refinement details for the PD2 and PD1 quasicrystal approximant structures.

of all reflections has been done. For the determination of space group, the two-dimensional slices cut from the 3D-RED data along the (*hk*0), (*h*0*l*), and (0*kl*) planes were used to derive the extinction conditions. The final file produced with *hkl* intensity was used for solving the structure by standard crystallographic techniques. Based on RED intensities, the structure was solved by direct methods and refined using the program *SHELX*97 [59, 60]. Nearly all atoms could be located and refined isotropically using the RED data. The simulated electron diffraction patterns were calculated using the intensities obtained from the output of *SHELX*97.

3. Structure analysis of PD2 and PD1 quasicrystal approximants

3.1 RED data processing

The 3D reciprocal space can be obtained by combining the series of electron diffraction frames. RED data processing program is used for the reciprocal space reconstruction of the electron diffraction data. The unit cell dimensions for PD2 and PD1 were found to be a = 23.2, b = 32.3, c = 4.1 Å, angles α = 89.7, β = 90.1, γ = 89.3° (**Figure 2**) and a = 37.3, b = 38.8, c = 8.2 Å, α = 89.9, β = 90.1, γ = 90.1°, respectively, indicating that both PD2 and PD1 are orthorhombic (**Table 1**). We present here only the RED images of the PD2 quasicrystal approximant. For the RED images of PD1, we refer the readers to the reference [42]. The entire 3D reciprocal lattice of PD2 obtained from the 3D-RED data viewed along c^* is shown in **Figure 2(a)**. Only the data out to 1.0 Å are shown because the reflections outside 1.0 Å were too weak to be detected and the completeness was too low. The presence of several 10-fold rings can be seen. The c lattice parameter is described as either 4.1 or 8.2 Å. The longer c-axis dimension (8.2 Å) can be considered as the cell parameter of a superstructure.

Figure 2(b) shows the original data set projected along b^*; the 8.2 Å layers are seen. The odd layers (corresponding to the 8.2 Å c axis, shown in red) are much weaker than the even layers (corresponding to a 4.1 Å c axis). For a = 46.4, b = 64.6, and c = 8.2 Å, the space group was found to be *F*222 (No. 22), *F*2*mm* (No. 42), or *Fmmm* (No. 69). However, it is possible to treat the structure as having a c-axis of 4.1 Å. Since the total intensities of reflections with even l indices are more than four

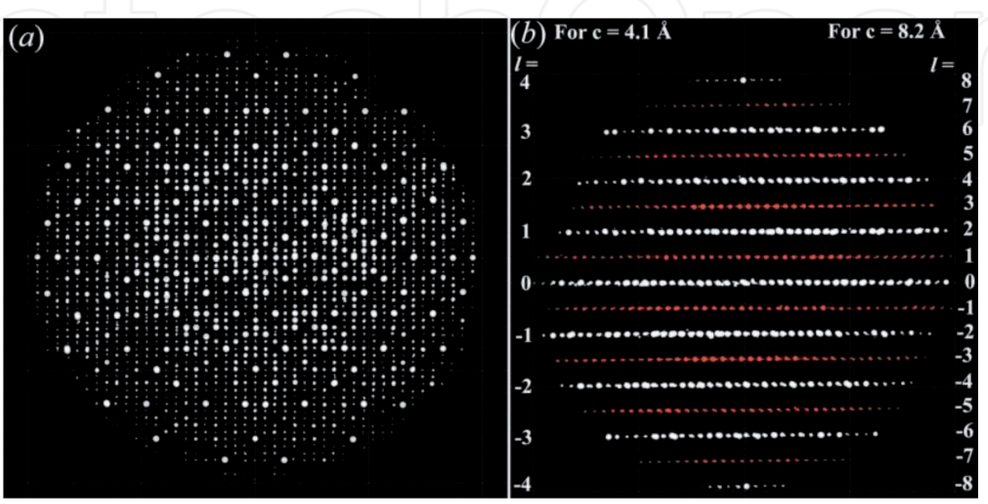

Figure 2.
(a) The entire 3D reciprocal lattice of PD2 obtained from the 3D-RED data viewed along c. (b) the original data set projected along b*. the odd layers (corresponding to the 8.2 Å c-axis, shown in red) are much weaker than the even layers (corresponding to a 4.1 Å c axis). Reproduced with permission of the International Union of Crystallography (https://scripts.iucr.org/cgi-bin/paper?HE5621) [41].*

times higher than those with odd l indices for c = 8.2 Å; the basic structure, i.e., using c = 4.1 Å, has been solved by only considering the reflections of even l indices. The axes a and b are selected in such a way so that the diffraction spot present at 2.0 Å resolution is along b^* and the equally strong diffraction spot present at 2.3 Å resolution is along a^* (**Figure 3**).

Figure 4(a)–(c) show the 2D slices ($hk0$), ($h0l$), and ($0kl$) of the reconstructed reciprocal lattice obtained from the 3D-RED data. Each slice corresponds to one complete quadrant for orthorhombic compounds containing all unique reflections. The missing reflections attributed to the missing cone. The odd layers (corresponding to the 8.2 Å c-axis, shown in red colour in (b) and (c)) are much weaker than the even layers (corresponding to a 4.1 Å c-axis).

Figure 5(a)–(c) show 2D slices of ($hk1$) and ($hk-1$), ($hk2$) and ($hk-2$), and ($hk3$) and ($hk-3$) corresponding to c = 4.1 Å. Two layers of each are combined and shown together. The white reflections correspond to hkl, while yellow corresponds to $hk-l$ layers. The corresponding calculated kinematical electron diffraction patterns agree very well (**Figure 5(d)–(f)**). Notice the presence of many rings of 10 strong reflections. This is typical of 10-fold quasicrystals and their approximants.

3.2 Solving the basic atomic structure and deducing an atomic model of PD2 and PD1

Based on the systematic absences for the unit cell with c = 4.1 Å for PD2 ($0kl$: $k + l = 2n + 1$; $0\,k0$: $k = 2n + 1$; $00\,l$: $l = 2n + 1$) and PD1 ($0kl$: $k + l = 2n$; $h0l$: $h = 2n$; $h00$: $h = 2n$; $0\,k0$: $k = 2n$; $00\,l$: $l = 2n$), the space groups were found to be [*Pnmm* (No. 59) or $Pnm2_1$ (No. 31)] for PD2 and [*Pnam* (No. 62) or $Pna2_1$ (No.33)] for PD1. *Pnmm* and *Pnam* are centrosymmetric and have a higher symmetry than $Pnm2_1$ and $Pna2_1$. Since most inorganic structures are centrosymmetric, thus the PD2 and PD1 structures were first solved in *Pnmm* and *Pnam*, respectively.

Since the procedure followed for the structure solution and refinement using RED data is same for both the structures, we discuss here only the step-by-step

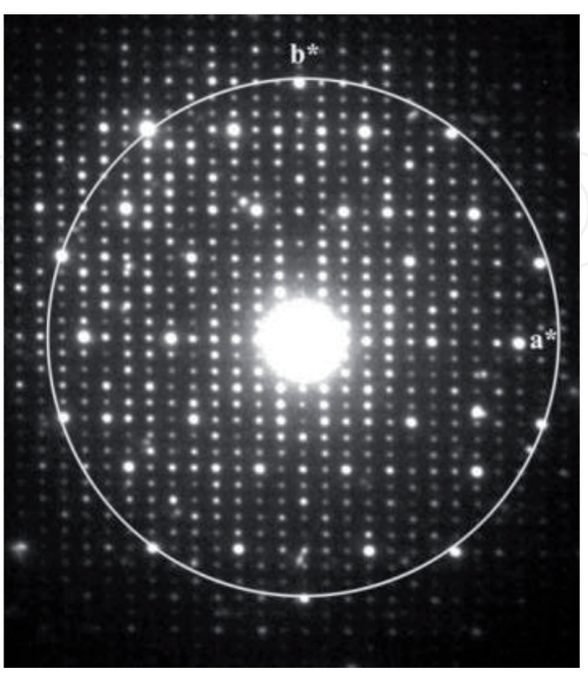

Figure 3.
Selected area electron diffraction pattern of the hk0 layer of PD2. This electron diffraction pattern was collected on a JEOL JEM-2000FX microscope. Reproduced with permission of the International Union of Crystallography (https://scripts.iucr.org/cgi-bin/paper?HE5621) [41].

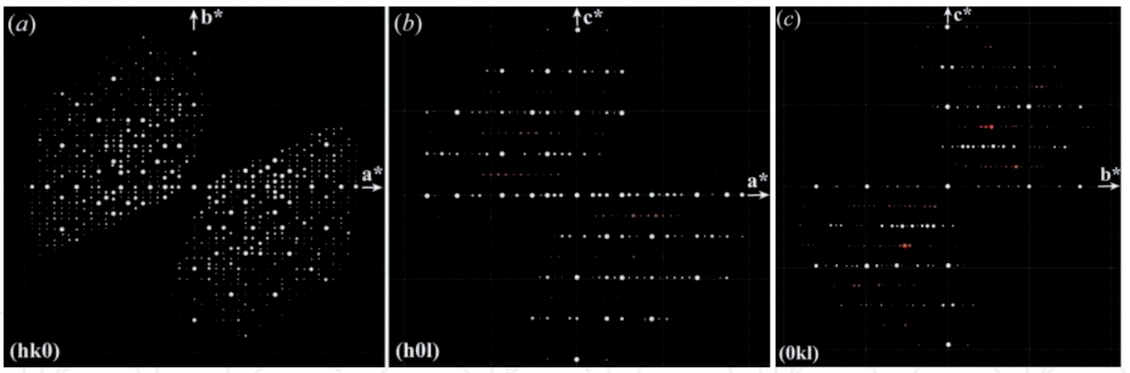

Figure 4.
Two-dimensional slices of the reconstructed reciprocal lattice obtained from the 3D-RED data. (a) (hk0), (b) (hol), and (c) (okl). The layers shown in red colour in (b) and (c) for c = 8.2 Å are much weaker than the even layers of c = 4.1 Å. reproduced with permission of the International Union of Crystallography (https://scripts.iucr.org/cgi-bin/paper?HE5621) [41].

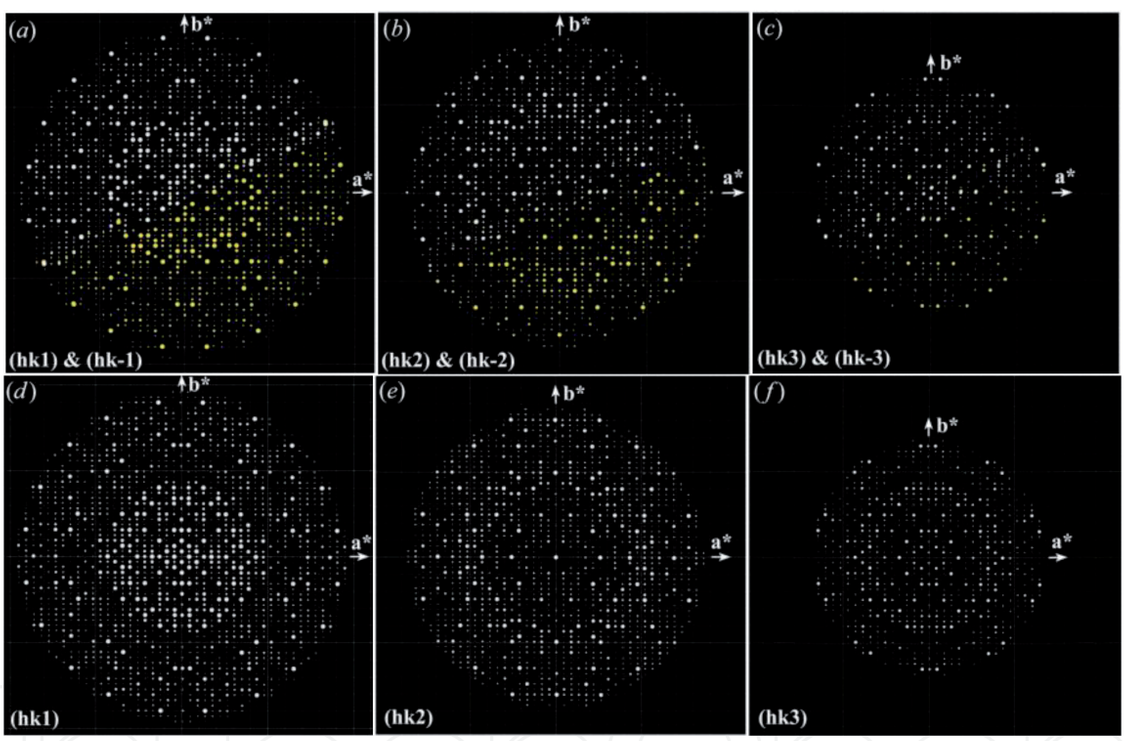

Figure 5.
(a)–(c) 2D slices of (hk1) and (hk − 1), (hk2) and (hk − 2), and (hk3) and (hk-3) for c = 4.1 Å obtained from experimental RED data. Here, two layers of each are combined and shown together. The white reflections correspond to hkl while yellow corresponds to hk − l layers. (d)–(f) simulated kinematical electron diffraction patterns after the final refinement of the structure model using c = 4.1 Å [(hk1), (hk2) and (hk3), respectively]. Reproduced with permission of the International Union of Crystallography (https://scripts.iucr.org/cgi-bin/paper?HE5621) [41].

details in the structure determination of PD2 structure. The details for the PD1 structure is reported elsewhere [42]. The crystallographic data, RED experimental parameters, and structure refinement details for the PD2 and PD1 structures are given in **Table 1**. In the case of PD2, a total of 8153 reflections, of which 1799 are unique, within 1.0 Å resolution, were collected. The structure model of PD2 was deduced by direct methods using *SHELX*97. The refinement of structure was done by taking the square root of the intensities as an estimate for the standard deviation (σ). The final structure refinement with the 3D-RED data converged to $R_1 = 0.43$ for the 1799 unique reflections (89.3% of all unique reflections up to $d \geq 1.0$ Å were observed above the background noise level). From the structure solution, the

first 26 highest unique peaks (atoms) found by *SHELX* were examined. Two 2 nm wheels were clearly seen per unit cell. There are three concentric rings of atoms in each wheel: innermost 5, then 10, and finally 20 arranged in 10 pairs. These three rings comprise of total 17 unique atoms. These 17 atoms are considered as Co/Ni atoms. In the periodic table, Co and Ni lie adjacent to each other and thus cannot be distinguished by the present technique. The nine remaining peaks were assigned to Al. They can be seen at several places in the unit cell but did not form patterns of fivefold symmetry. In one 2 nm wheel cluster, the five innermost atoms have the same z coordinate (in *Pnmm,* because of the short c-axis, all atoms must be located at one of the two mirror planes $z = 0.25$ or $z = 0.75$). In the next ring the 10 Co/Ni atoms are arranged in an alternate manner at $z = 0.25$ and 0.75 (**Figure 6(c)**). At the rim of the 2 nm wheel cluster, the 20 atoms are arranged in pairs when viewed along the c-axis. One atom is at $z = 0.25$ and the other at $z = 0.75$ in each such pair. For any two such pairs, the nearest atoms in adjacent pairs are at the same height, i.e., either both are at $z = 0.25$ or both are at $z = 0.75$. The assigned 17 atoms as Co/Ni correspond to the 14 highest peaks and peaks 16, 19, and 21. Thus only four of the highest peaks, i.e., 15, 17, 18 and 20, were considered to arise from Al.

Comparing the structure model of PD2 generated by *SHELXS*97 with that of PD4, which was obtained from single-crystal X-ray diffraction [37], we found a one-to-one agreement for all the 35 Co/Ni atoms in the 2 nm wheels. This similarity is not limited to the projected structure; all the coordinates of z also agree between PD2 and PD4. In the region of small hour glass shaped between two

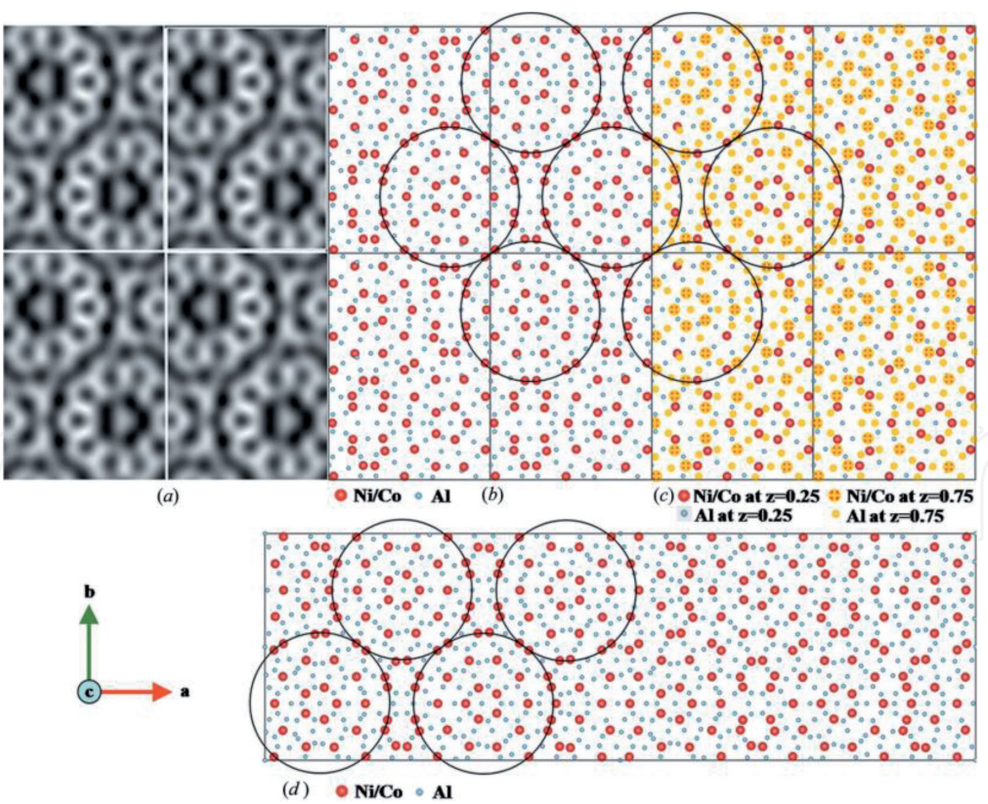

Figure 6.
(a) HRTEM image of PD2 with 2 × 2 unit cells taken along the c axis [39]. The 10-fold wheels containing atoms (in black color) are clearly seen. (b) the PD2 atomic structure model projected along the c-axis. The 2 nm wheel cluster columns with pseudo 10-fold rotational symmetry are shown by circles. Co/Ni atoms are shown in red color while Al atoms in blue. (c) the Co/Ni atoms at z = 0.25 (red) and z = 0.75 (red with yellow cross) layers are shown in the structure model. (d) the structure of PD4 (a = 101.3, b = 32.0, c = 4.1 Å) as determined by X-ray crystallography [37]. The circles mark the 2 nm clusters similar to those found in PD2. Reproduced with permission of the International Union of Crystallography (https://scripts.iucr.org/cgi-bin/paper?HE5621) [41].

non-intersecting wheels, there were no Co/Ni atoms. After finding all the 35 Co/Ni atoms, we started observing for the Al atoms among the *Q* peaks in the difference Fourier maps generated by *SHELX*. After each refinement step, the stability of the atoms in the structure model was checked. The atomic displacements after the refinement did not show significant movements. We have found 55 unique atomic positions (17 Co/Ni and 38 Al) in the unit cell with a reasonable geometry after refinement using *SHELXL*97. This is close to the nominal and experimentally determined (by EDS) chemical composition except that one or two Al atoms may still be missing from our model. The structure model was also deduced using the strong reflections approach [61] which is quite similar to that obtained by direct methods. **Figure 6(b)** and **(c)** shows the structure model of PD2 obtained from the RED data. The high value of R_1 (43%) is normal for data obtained from electron diffraction. This high value may come from twins and intergrowth with other approximants in the PD series, especially for PD1. It partly also arises due to the distortions of the intensities by multiple scattering. The PD4 also had a remarkably high R-value (24.5%), even though it was solved from single-crystal X-ray diffraction data. After the final refinement of PD2, the chemical composition calculated was found to be $Al_{37}(Co/Ni)_{15.5}$. The atomic structure shown here agrees well with the lower resolution structure model obtained from HRTEM images [39]. **Figure 6(a)** shows an experimental HRTEM image of PD2 taken along the *c*-axis after applying crystallographic image processing using *CRISP* [62]. The plane group symmetry was found to be *pgg* for PD2. The transition metal atoms are black in color with 10-fold wheels are clearly seen. The wheels are 23.2 Å apart (along *a*), while vertically (along *b*) they are 32.2 Å apart, and they are intersecting diagonally at 19.8 Å. As shown in **Figure 6**, the projected unit cell consists of circular wheel clusters of 2 nm in diameter. Around the perimeters of each of the 2 nm cluster columns, dark spots belonging to Co and Ni atoms appear.

Figure 6(c) shows the atomic arrangement in the $z = 0.25$ and $z = 0.75$ layers. Some of the atoms which appear to be very close to each other in projection are actually separated by 2.05 Å along *z*. The 5 Co/Ni and 5 Al atoms which form the pentagons in the circular wheel cluster are present in different layers. Outside the pentagon, there are three circular arrangements of atoms. There are 10 Al and 10 Co/Ni atoms in the first and second circles, respectively. The atoms present in these circles at $z = 0.25$ are followed by atoms at $z = 0.75$ and vice versa. Thus, this leads to the formation of systematic circular sequence of atoms present in different layers. The third circle consists of 10 pairs of Co/Ni atoms. The intersecting wheels share four Co/Ni atoms from two pairs, thus locking in the wheel positions relative to each other. Simulated electron diffraction patterns are produced using the intensities found from the output of *SHELX*97 after the final refinement for the structure model. The simulated electron diffraction patterns generated are found to be in good agreement with experimental electron diffraction patterns (**Figure 5**). The simulated electron diffraction patterns show the presence of 10-fold symmetry.

A total of 7070 reflections were collected for the PD1 structure. Out of which 2588 are unique. The data completeness is 94.5% for the reflections with $d \geq 1.0$ Å. The R_{int} value is found to be 0.26, which is much higher than that for single-crystal X-ray diffraction but normal for electron diffraction data. The causes for this relatively poor data quality compared to single-crystal X-ray diffraction are currently under investigation. The program *SHELXL* was used for structure refinement. The final structure refinement for the 3D-RED data converged to $R_1 = 0.36$ without using any geometric restraints. **Figure 7(b)** shows the structure model of PD1 obtained from RED data. **Table 1** gives the crystallographic data, RED experimental parameters, and structure refinement details for the PD1 structure model. Successive refinement using *SHELXL* gives in 108 unique atomic positions

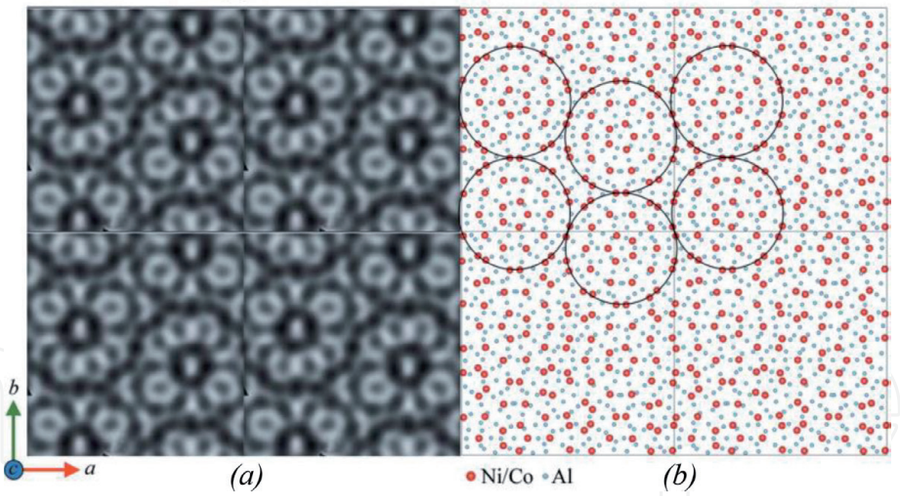

Figure 7.
(a) HRTEM image of PD1 with 2 × 2 unit cells, taken along the c axis [39]. Transition metal atoms appear as black regions around the perimeters of each of the 2 nm wheel clusters. (b) Atomic structure model of PD1 obtained by RED after final refinement, projected along the c-axis. Reproduced with permission of the International Union of Crystallography (https://scripts.iucr.org/cgi-bin/paper?jo5016) [42].

(31 Co/Ni and 77 Al) all with a reasonable geometry. After the refinement of PD1, the chemical composition calculated was found to be $Al_{77}(Co/\ Ni)_{31}$, which is close to the nominal and experimental chemical composition determined by EDS, except that a few Al atoms may still be missing from our model. The PD1 structure (108) has almost twice as many unique atoms as that of PD2 (55). The structural model presented here agrees well with the experimental HRTEM image of PD1 [39]. The HRTEM image of PD1 (taken along the *c*-axis) after applying crystallographic image processing using *CRISP* is shown in **Figure 7(a)**. The plane-group symmetry was found to be *pgg* for PD1. The 2 nm wheels are clearly seen. As shown in **Figure 8(a)** and **(b)** for PD1 and PD2, the atoms present at the layers $z = 0.25$ and $z = 0.75$ form systematic circular sequences. At the center of each wheel, five Co/Ni

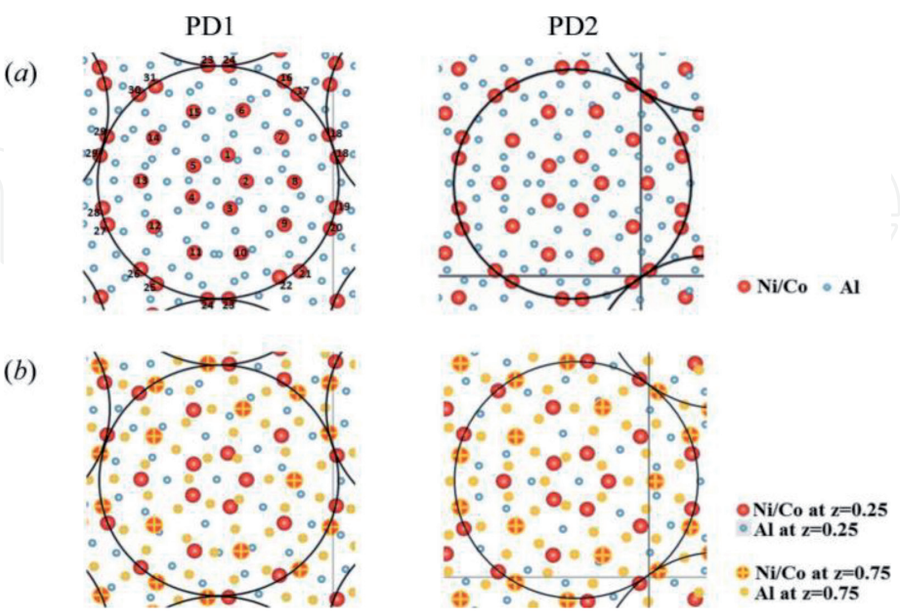

Figure 8.
(a) Circular wheel clusters of PD1 with PD2 obtained from RED data are compared. (b) PD1 and PD2 show identical arrangements of Ni/Co atoms present at z = 0.25 (red) and z = 0.75 (red with yellow cross) within the wheel cluster. Although, most of the Al atoms appear in similar locations within the wheels in PD1 and PD2, there are some differences. Reproduced with permission of the International Union of Crystallography (https://scripts.iucr.org/cgi-bin/paper?jo5016) [42].

and five Al atoms present in different layers form pentagons. There are four circular arrangements of atoms outside these pentagons. There are 10 Al atoms in the first circle, 10 Co/Ni and nearly 20 Al atoms in the second circle, nearly 30 Al atoms in the third circle, and 10 pairs of Co/Ni atoms and just a few Al atoms in the fourth and outermost ring. In all these circles, the atoms present at $z = 0.25$ are followed by atoms at $z = 0.75$ in a very regular fashion quite similar in PD1 and PD2.

The positions for all stronger Co/Ni scatterers are correct, while the positions of weaker Al scatterers are more uncertain. As discussed earlier, few Al atoms may be missing, few may be misplaced, and several may have split occupancies or could be shared Al/Co and/or Al/Ni sites. With the present data quality of electron diffraction, such fine details cannot be determined unambiguously. Some work has been done and some in progress on the ways to compensate the problems with respect to quality of data and absorption that combine to give electron diffraction intensity data that are inferior to those collected by X-ray diffraction. In the present case, the structure refinement can be done, and at least the Co/Ni atoms were found to be stable during refinement. The arrangement of Co/Ni atoms is in excellent agreement with previous studies by single-crystal X-ray diffraction for PD8 [38] and PD4 [37] and with the low-resolution projections obtained by HRTEM on PD1 [39].

4. Conclusions

Based on the results described and discussed in this chapter, it is proven that rotation electron diffraction method is an effective method to solve the structures of a rather complex and dense quasicrystal approximants. The structural details of pseudo-decagonal (PD) quasicrystal approximants PD2 and PD1 discussed in this chapter helped us to understand the atomic arrangements within the 2 nm wheel clusters. These are one of the most complex structures ever solved to atomic resolution by electron diffraction. The structural models obtained from the RED data agree well with the high-resolution transmission electron microscopy images.

Acknowledgements

One of the author (D. Singh) gratefully acknowledges the financial support by Department of Science and Technology (DST), New Delhi, India, in the form of INSPIRE Faculty Award [IFA12-PH-39]. The authors thank the Swedish Research Council (VR), the Swedish Governmental Agency for Innovation Systems (VINNOVA), and the Knut and Alice Wallenberg Foundation for the financial support through the project grant 3DEM-NATUR.

Author details

Devinder Singh[1*] and Sven Hovmöller[2]

1 Amity School of Applied Sciences, Amity University, Lucknow, UP, India

2 Department of Materials and Environmental Chemistry, Stockholm University, Stockholm, Sweden

*Address all correspondence to: dsingh2@lko.amity.edu

IntechOpen

References

[1] Zhang D, Oleynikov P, Hovmöller S, Zou XD. Collecting 3D electron diffraction data by the rotation method. Zeitschrift fuer Kristallographie. 2010;**225**:94-102

[2] Zou XD, Hovmöller S, Oleynikov P. Electron Crystallography: Electron Microscopy and Electron Diffraction. Oxford, England, UK: International Union of Crystallography, Oxford Science Publications; 2011. ISBN: 978-0-19-958020-0, Chapter 11

[3] Willhammar T, Sun J, Wan W, Oleynikov P, Zhang D, Zou XD, et al. Structure and catalytic properties of the most complex intergrown zeolite ITQ-39 determined by electron crystallography. Nature Chemistry. 2012;**4**:188-194

[4] Wan W, Sun J, Su J, Hovmöller S, Zou XD. Three-dimensional rotation electron diffraction: Software RED for automated data collection and data processing. Journal of Applied Crystallography. 2013;**46**:1863-1873

[5] Martínez-Franco R, Moliner M, Yun Y, Sun J, Wan W, Zou XD, et al. Synthesis of an extra-large molecular sieve using proton sponges as organic structure-directing agents. Proceedings of the National Academy of Sciences of the United States of America. 2013;**110**:3749-3754

[6] Su J, Kapaca E, Liu L, Georgieva V, Wan W, Sun J, et al. Structure analysis of zeolites by rotation electron diffraction (RED). Microporous and Mesoporous Materials. 2013;**189**:115-125

[7] Yadav TP, Singh D, Tiwari RS, Srivastava ON. Enhanced microhardness of mechanically activated carbon–quasicrystal composite. Materials Letters. 2012;**80**:5-8

[8] Singh D, Mandal RK, Tiwari RS, Srivastava ON. Nanoindentation characteristics of $Zr_{69.5}Al_{7.5-x}Ga_xCu_{12}Ni_{11}$ glasses and their nanocomposites. Journal of Alloys and Compounds. 2011;**509**:8657-8663

[9] Singh D, Yadav TP, Mandal RK, Tiwari RS, Srivastava ON. Effect of Ga substitution on the crystallization behaviour and glass forming ability of Zr–Al–Cu–Ni alloys. Materials Science and Engineering A. 2010;**527**:469-473

[10] Singh D, Yadav TP, Mandal RK, Tiwari RS, Srivastava ON. Indentation characteristics of metallic glass and nanoquasicrystal-glass composite in Zr–Al(Ga)–Cu–Ni alloys. Intermetallics. 2010;**18**:2445-2452

[11] Singh D, Yadav TP, Mandal RK, Tiwari RS, Srivastava ON. Effect of Ti addition on the quasicrystalline phase formation and indentation characteristics of $Zr_{69.5}Al_{7.5}Cu_{12}Ni_{11}$ alloy. Philosophical Magazine. 2011;**91**:2837

[12] Singh D, Singh D, Yadav TP, Mandal RK, Tiwari RS, Srivastava ON. Synthesis and indentation behavior of amorphous and nanocrystalline phases in rapidly quenched Cu–Ga–Mg–Ti and Cu–Al–Mg–Ti alloys. Metallography, Microstructure, and Analysis. 2013;**2**:321-327

[13] Singh D, Yadav TP, Mandal RK, TiwariRS,SrivastavaON.Nanoindentation studies of metallic glasses and nanoquasicrystal glass composites in ZrAl(Ga)CuNi alloys. International Journal of Nanoscience. 2011;**10**:929-933

[14] Shechtman D, Blech I, Gratias D, Cahn J. Metallic phase with long-range orientational order and no translational symmetry. Physical Review Letters. 1984;**53**:1951-1953

[15] Somekawa H, Watanabe H, Mukai T. Damping properties in

Mg–Zn–Y alloy with dispersion of quasicrystal phase particle. Materials Letters. 2011;**65**:3251-3253

[16] Dubois J. So useful, those quasicrystals. Israel Journal of Chemistry. 2011;**51**:1168-1175

[17] Singh D, Shahi RR, Yadav TP, Mandal RK, Tiwari RS, Srivastava ON. Hydrogenation of $(Zr_{69.5}Al_{7.5}Cu_{12}Ni_{11})_{100-x}Ti_x$ quasicrystalline alloys and its effect on their structural and microhardness behaviour. Journal of Non-Crystalline Solids. 2013;**380**:11

[18] Yadav TP, Singh D, Shahi RR, Shaz MA, Tiwari RS, Srivastava ON. Formation of quasicrystalline phase in $Al_{70-x}Ga_xPd_{17}Mn_{13}$ alloys. Philosophical Magazine. 2011;**91**:2474

[19] Singh D, Singh D, Mandal RK, Srivastava ON, Tiwari RS. Crystallization behavior and mechanical properties of $(Al_{90}Fe_5Ce_5)_{100-x}Ti_x$ amorphous alloys. Journal of Alloys and Compounds. 2016;**687**:990-998

[20] Yadav TP, Singh D, Shaz MA, Tiwari RS, Srivastava ON. Synthesis of quasicrystalline film of Al–Ga–Pd–Mn alloy. Thin Solid Films. 2013;**534**:265

[21] Singh D, Singh D, Srivastava ON, Tiwari RS. Microstructural effect on the low temperature transport properties of Ce–Al (Ga) metallic glasses. Scripta Materialia. 2016;**118**:24-28

[22] Goldman A, Kelton R. Quasicrystals and crystalline approximants. Reviews of Modern Physics. 1993;**65**:213-230

[23] Cahn JW, Gratias D, Shechtman D. Pauling's model not universally accepted. Nature. 1986;**319**:102-103

[24] Duneau M, Mosseri R, Oguey C. Approximants of quasiperiodic structures generated by the inflation mapping. Journal of Physics A. 1989;**22**:4549-4564

[25] Singh D, Tiwari RS, Srivastava ON. Phase formation in rapidly quenched Cu-based alloys. Journal of Materials Science. 2009;**44**:3883-3888

[26] Bancel PA. Dynamical phasons in a perfect quasicrystal. Physical Review Letters. 1989;**63**:2741-2744

[27] Abe E, Tsai A. Quasicrystal-crystal transformation in Zn–Mg-rare-earth alloys. Physical Review Letters. 1999;**83**:753-756

[28] Zou X, Fung K, Kuo K. Orientation relationship of decagonal quasicrystal and tenfold twins in rapidly cooled Al–Fe alloy. Physical Review B. 1987;**35**:4526-4528

[29] Singh D, Hovmöller S, Grushko B, Wan W, Yun Y, Zou XD. A complex pseudo-decagonal quasicrystal approximant solved by strong reflections approach. Acta Crystallographica Section A. 2017;**A73**:c1192

[30] Hovmöller S, Singh D, Grushko B, Wan W, Yun Y, Zou XD. A complex pseudo-decagonal quasicrystal approximant solved by the strong reflections approach and refined against rotation electron diffraction (RED) data. Acta Crystallographica Section A. 2016;**A72**:s318

[31] Hovmöller S, Singh D, Wan W, Yun Y, Wan W, Grushko B, et al. Quasicrystal approximants solved by rotation electron diffraction (RED). Acta Crystallographica Section A. 2014;**A70**:c1195

[32] Hiraga K, Sun W, Ohsuna T. Structure of a pentagonal quasicrystal in $Al_{72.5}Co1_{7.5}Ni_{10}$ studied by high-angle annular detector dark-field scanning transmission electron microscopy. Materials Transactions, JIM. 2001;**42**:1146-1148

[33] Hiraga K, Ohsuna T, Yubuta K, Nishimura S. The structure of an

Al–Co–Ni crystalline approximant with an ordered arrangement of atomic clusters with pentagonal symmetry. Materials Transactions, JIM. 2001;**42**:897-900

[34] Saitoh K, Tsuda K, Tanaka M. New structural model of an $Al_{72}Ni_{20}Co_8$ decagonal quasicrystal. Journal of the Physical Society of Japan. 1998;**67**:2578-2581

[35] Grushko B, Holland-Moritz D, Wittmann R, Wilde G. Transition between periodic and quasiperiodic structures in Al–Ni–Co. Journal of Alloys and Compounds. 1998;**280**:215-230

[36] Döblinger M. PhD thesis. Berlin, Germany: University of Karlsruhe, Logos Verlag; 2002

[37] Oleynikov P, Demchenko L, Christensen J, Hovmöller S, Yokosawa T, Döblinger M, et al. Structure of the pseudodecagonal Al–Co–Ni approximant PD4. Philosophical Magazine. 2006;**86**:457-462

[38] Sugiyama K, Nishimura S, Hiraga K. Structure of a W–(AlCoNi) crystalline phase related to Al–Co–Ni decagonal quasicrystals, studied by single crystal X-ray diffraction. Journal of Alloys and Compounds. 2002;**342**:65-71

[39] Hovmöller S, Zou L, Zou XD, Grushko B. Structures of pseudo-decagonal approximants in Al–Co–Ni. Philosophical Transactions of the Royal Society of London. Series A. 2012;**370**:2949-2959

[40] Estermann MA, Lemster K, Steurer W, Grushko B, Döblinger M. Structure solution of a high-order decagonal approximant $Al_{71}Co_{14.5}Ni_{14.5}$ by maximum entropy Patterson deconvolution. Ferroelectrics. 2001;**250**:245-248

[41] Singh D, Yun Y, Wan W, Grushko B, Hovmöller S, Zou XD. A complex pseudo-decagonal quasicrystal approximant $Al_{37}(Co,Ni)_{15.5}$ solved by the rotation electron diffraction (RED) method. Journal of Applied Crystallography. 2014;**47**:215

[42] Singh D, Yun Y, Wan W, Grushko B, Hovmöller S, Zou XD. Structure determination of a pseudo-decagonal quasicrystal approximant by the strong-reflections approach and rotation electron diffraction. Journal of Applied Crystallography. 2016;**49**:433-441

[43] Guyot P, Audier M. A quasicrystal structure model for Al–Mn. Philosophical Magazine B. 1985;**52**:L15-L19

[44] Elser V, Henley CL. Crystal and quasicrystal structures in Al–Mn–Si alloys. Physical Review Letters. 1985;**55**:2883-2886

[45] Steurer W. Five-dimensional Patterson analysis of the decagonal phase of the system Al–Mn. Acta Crystallographica Section B. 1989;**45**:534-542

[46] Jeong HC, Steinhardt PJ. Cluster approach for quasicrystals. Physical Review Letters. 1994;**73**:1943-1946

[47] Hiraga K, Lincoln FJ, Sun W. Structure and structural change of Al–Ni–Co decagonal quasicrystal by high-resolution electron microscopy. Materials Transactions, JIM. 1991;**32**:308-314

[48] Saitoh K, Tsuda K, Tanaka M, Tsai AP, Inoue A, Masumoto T. Electron microscope study of the symmetry of the basic atom cluster and a structural change of decagonal quasicrystals of Al–Cu–Co alloys. Philosophical Magazine A. 1996;**73**:387-398

[49] Saitoh K, Tsuda K, Tanaka M, Kaneko K, Tsai AP. Structural study of an $Al_{72}Ni_{20}Co_8$ decagonal quasicrystal

using the high-angle annular dark-field method. Japanese Journal of Applied Physics. 1997;**36**:L1400-L1402

[50] Tsuda K, Nishida Y, Saitoh K, Tanaka M, Tsai AP, Inoue A, et al. Structure of Al–Ni–Co decagonal quasicrystals. Philosophical Magazine A. 1996;**74**:697-708

[51] Ritsch S. Highly perfect decagonal Al–Co–Ni quasicrystals. Philosophical Magazine Letters. 1996;**74**:99-106

[52] Steurer W, Kuo KH. Five-dimensional structure analysis of decagonal $Al_{65}Cu_{20}Co_{15}$. Acta Crystallographica Section B. 1990;**46**:703-712

[53] Burkov SE. Structure model of the Al–Cu–Co decagonal quasicrystal. Physical Review Letters. 1991;**67**:614-617

[54] Yamamoto A. Science Reports of the Research Institutes, Tohoku University, Series A. 1996;**42**:207-212

[55] Saitoh K, Tsuda K, Tanaka M. Structural models for decagonal quasicrystals with pentagonal atom-cluster columns. Philosophical Magazine A. 1997;**76**:135-150

[56] Cockayne E, Widom M. Ternary model of an Al–Cu–Co decagonal quasicrystal. Physical Review Letters. 1998;**81**:598-601

[57] Deloudi S, Fleischer F, Steurer W. Unifying cluster-based structure models of decagonal Al–Co–Ni, Al–Co–Cu and Al–Fe–Ni. Acta Crystallographica Section B. 2011;**67**:1-17

[58] Wan W, Sun JL, Hovmöller S, Zou XD. RED data collection and data processing. 2013. Available from: http://www.calidris-em.com

[59] Sheldrick GM. In: Fortier S, editor. Direct Methods for Solving Macromolecular Structures. Dordrecht: Kluwer Academic Publishers; 1998. pp. 401-411

[60] Sheldrick GM. A short history of *SHELX*. Acta Crystallographica Section A. 2008;**64**:112-122

[61] Christensen J, Oleynikov P, Hovmöller S, Zou XD. Solving approximant structures using a "strong reflections" approach. Ferroelectrics. 2004;**305**:273-277

[62] Hovmöller S. *CRISP*: Crystallographic image processing on a personal computer. Ultramicroscopy. 1992;**41**:121-135